Korean J Physiol Pharmacol
Vol 13: 55−59, February, 2009

Quantitative Structure Activity Relationship between Diazabicyclo-[4.2.0]octanes Derivatives and Nicotinic Acetylcholine Receptor Agonists

Eun Ae Kim, Kyoung Chul Jung, Uy Dong Sohn, and Chaeuk Im

College of Pharmacy, Chung-Ang University, Seoul 156-756, Korea

Three dimensional quantitative structure activity relationship between diazabicyclo[4.2.0]octanes and nicotinic acetylcholine receptor (h$\alpha 4\beta 2$ and h$\alpha 3\beta 4$) agonists was studied using comparative molecular field analysis (CoMFA) and comparative molecular similarity indices analysis (CoMSIA). From 11 CoMFA and CoMSIA models, CoMSIA with steric and electrostatic fields gave the best predictive models (q^2=0.926 and 0.945, r^2_{ncv}=0.983 and 0.988). This study can be used to develop potent h$\alpha 4\beta 2$ receptor agonists with low activity on h$\alpha 3\beta 4$ subtype.

Key Words: Diazabicyclo[4.2.0]octanes, CoMFA, CoMSIA, Nicotinic acetylcholine receptors (nAChRs)

INTRODUCTION

The nicotinic acetylcholine receptors (nAChRs) are ligand-gated ion channels widely distributed in central nervous system (CNS) (Hogg & Bertrand, 2004; Cashin et al, 2007; Lape et al, 2008). The agonists bind to nAChR receptors and result in conformational change of the receptors, which lead to channel opening for the permeation of Na^+ ion. They mediate acetylcholine (Ach) neurotransmission and adjust the activities of neurotransmitters such as dopamine, serotonin, glutamate, and GABA (Girod et al, 2000; Kenny et al, 2000; Dehkordi et al, 2007; Grady et al, 2007). These receptors are associated with diseases such as epilepsy, cognition disorders, Alzheimer's diseases, Parkinson's diseases, and nicotine addiction (Dougherty et al, 2003; Vincler & McIntosh, 2007; Hays et al, 2008; Kuryatov et al, 2008; Owen et al, 2008; O'Leary et al, 2008; Pons et al, 2008). The nAChRs can be classified according to several subunits. The major subtype of nAChRs in the CNS is $\alpha 4\beta 2$, whereas the $\alpha 3\beta 4$ subtype is found mainly in the peripheral nervous system (Jensen et al, 2005; Gotti et al, 2006).

The $\alpha 4\beta 2$ subtype has become an important therapeutic target for analgesics, while the activity at the $\alpha 3\beta 4$ subtype is known to be related to the side effects on gastrointestinal and cardiovascular systems. The 3,8-diazabicyclo[4.2.0]octane compounds are very active analgesics, and some of them show nanomolar potency in the h$\alpha 4\beta 2$ receptor subtype. However, they are not selective for $\alpha 4\beta 2$ over $\alpha 3\beta 4$ subtypes (Frost et al, 2006).

From the quantitative structure - activity relationship (QSAR) studies, the characteristics of virtual receptor site and biological activity of unknown compounds can be predicted. Therefore, we have performed QSAR analysis to develop active compounds for $\alpha 4\beta 2$ but with low potency for $\alpha 3\beta 4$ subtypes, thereby which leading to potential analgesics with less side effects.

Corresponding to: Chaeuk Im, College of Pharmacy, Chung-Ang University, 221, Heuksuk-dong, Dongjak-gu, Seoul 156-756, Korea. (Tel) 82-2-820-5603, (Fax) 82-2-816-7338, (E-mail) Chaeukim@cau.ac.kr

METHODS

The 44 compounds with nicotinic acetylcholine receptor agonistic activity were taken from the literature for 3D-QSAR analysis, in which 37 compounds (1～37) were used for training set and 7 compounds (T1～T7) were selected for test set (Frost et al, 2006). The pEC_{50} ($-\log EC_{50}$) was calculated from the biological data (EC_{50}) and used in 3D-QSAR analysis. The structures of training and test sets are shown in Table 1 & 2.

Molecular modeling and alignment

All calculation was carried out using SYBYL 8.0 molecular modeling software (SYBYL, 2008). Molecular structures were sketched with sketch module in SYBYL and minimized by using TRIPOS force field with the Gasteiger Huckel charges and conjugated gradient method, and gradient convergence criteria of 0.05 kcal/mol. Simulated annealing on the energy minimized structures was performed with 50 cycles. They were heated at 2,000 K for 1,000 fs to reach the equilibrium and annealed to 200 K for 1,000 fs. The 50 conformations were then minimized to get low energy conformations for each compound.

The training set was aligned by using align database.

ABBREVIATIONS: nAChRs, nicotinic acetylcholine receptors; CNS, central nervous system; Ach, acetylcholine; GABA, γ -aminobutyric acid; 3D-QSAR, three dimensional quantitative structure activity relationship; pEC_{50}, -log EC_{50}; CoMFA, comparative molecular field analysis; CoMSIA, comparative molecular similarity indices analysis.

Table 1. Structures and biological activity of 3-N-substituted diazabicyclo[4.2.0]octanes

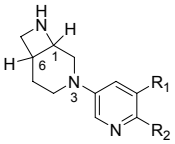

No	Stereoisomer	R_1	R_2	hα4β2 (EC_{50}, nM)	hα3β4 (EC_{50}, nM)
1	1R,6S	H	H	71	48
2	1S,6R	H	H	330	260
3	1R,6S	H	Cl	13	29
4	1S,6R	H	Cl	24	25
5	1R,6S	Br	H	150	76
6	1S,6R	Br	H	1,000	950
7	1R,6S	Cl	Cl	12	9.9
T1	1S,6R	Cl	Cl	82	110
8	1R,6S	Br	Br	7.8	8.2
9	1S,6R	Br	Br	76	110
10	1R,6S	CH_3	Cl	7.2	7.2
11	1S,6R	CH_3	Cl	47	71
T2	1R,6S	CN	H	1,900	1,000
12	1S,6R	CN	H	1,900	490
13	1R,6S	OMe	H	130	180
14	1S,6R	OMe	H	2,700	4,500
15	1R,6S	H	OMe	2,200	1,100
16	1S,6R	H	OMe	4,980	2,400
17	1R,6S	OEt	H	620	124
18	1S,6R	OEt	H	1,350	2,800
19	1S,6R	CH_3	H	650	1,400
T3	1R,6S	H	NO2	100	390
20	1S,6R	H	NO2	110	830
21	1R,6S	OMe	Br	21	8.0
22	1S,6R	OMe	Br	360	160
23	1R,6S	CN	Br	6.1	4.4
T4	1S,6R		H	180	5,700

This table is shown only for reader's convenience (*J Med Chem* 49: 7843−7853).

Table 2. Structures and biological activity of 8-N-substituted diazabicyclo[4.2.0]octanes

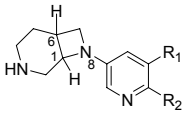

No	Stereoisomer	R_1	R_2	hα4β2 (EC_{50}, nM)	hα3β4 (EC_{50}, nM)
24	1R,6S	H	H	410	1,700
T5	1S,6R	H	H	1,400	1,540
25	1R,6S	H	Cl	37.4	1,390
26	1S,6R	H	Cl	216	1,520
27	1S,6R	Cl	Cl	176	339
T6	1R,6S	CH_3	Cl	76.1	1,910
28	1S,6R	CH_3	Cl	134	298
T7	1R,6S	OMe	Br	1,690	2,980
29	1S,6R	OMe	Br	200	202
30	1R,6S	CN	H	2,190	2,560
31	1S,6R	CN	H	1,930	5,560
32	1R,6S	CN	Br	109	794
33	1S,6R	CN	Br	172	238
34	1R,6S	$CONH_2$	Br	1,490	23,300
35	1S,6R	$CONH_2$	Br	340	7,460
36	1R,6S	OMe	H	7,690	63,500
37	1S,6R	OMe	H	1,105	4,360

This table is shown only for reader's convenience (*J Med Chem* 49: 7843−7853).

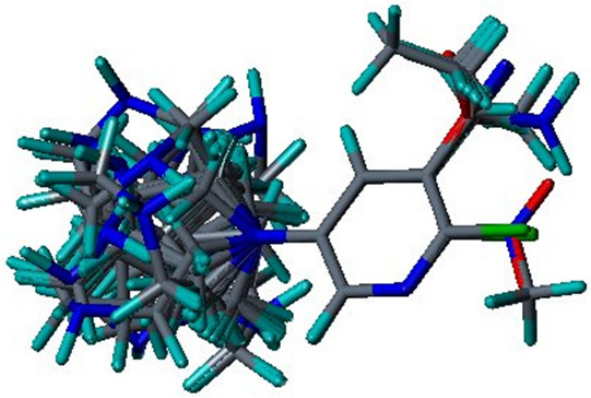

Fig. 1. The superimposed structures of aligned training set.

Compound (23) which showed the most potent activity was selected as template molecule, and pyridine moiety commonly found in all compounds was used for common substructure in alignment. The superimposed structures of aligned training set is shown in Fig. 1.

CoMFA and CoMSIA Analysis

In CoMFA analysis, steric and electrostatic fields were calculated with Lennard-Jones potential and Coulombic potential, respectively. The sp^3 carbon probe atom with +1.0 charge and Van der Waals radius of 1.52 A° was used to calculate the CoMFA steric and electrostatic fields. The cutoff values of the steric and electrostatic energies were 30.0 kcal/mol. In CoMSIA analysis, the probe atom with radius 1.0 A°, charge +1.0, hydrophobicity +1.0, hydrogen bond donating +1.0, and hydrogen bond accepting +1.0 were used to calculate similarity indices. An attenuation factor 0.3 was used to estimate the steric, electrostatic, hydrophobic, hydrogen bond donor, and acceptor fields in CoMSIA. The predictivity of the model was estimated by using leave one out (LOO) crossvalidation with SAMPLS, in which the highest q^2 value and the lowest standard error of prediction suggest the optimum number of components.

RESULTS

The statistical data from CoMFA and CoMSIA are shown in Table 3. For hα4β2 subtype model, statistical results from CoMSIA (0.926) with steric and electrostatic fields gave better q^2 than from CoMFA (0.892). The cross-validated value q^2 (0.926) and the non-cross-validated coefficient values r^2_{ncv} (0.983) indicate a good predictivity of

Table 3. CoMFA and CoMSIA results of the training set

Field*	$q^{2\dagger}$	N‡	SEP§	r^2_{ncv}‖	SEE¶	F**	Contributions				
							S	E	H	D	A
hα4β2 subtype											
CoMFA											
S	0.832	6	0.375	0.967	0.166	147.107	1				
E	0.819	6	0.390	0.966	0.168	143.232		1			
SE	0.892	6	0.301	0.987	0.104	382.064	0.534	0.466			
CoMSIA											
SE	0.926	6	0.249	0.983	0.120	285.165	0.128	0.872			
SEH	0.695	6	0.506	0.987	0.103	393.914	0.077	0.567	0.356		
SED	0.866	6	0.335	0.978	0.134	227.120	0.056	0.454		0.490	
SEA	0.884	6	0.312	0.978	0.136	220.764	0.117	0.782			0.101
SEDA	0.833	6	0.374	0.973	0.151	178.867	0.048	0.395		0.506	0.050
SEHD	0.595	1	0.608	0.980	0.129	248.687	0.046	0.339	0.199	0.415	
SEHA	0.650	6	0.542	0.986	0.110	344.311	0.067	0.422	0.356		0.156
SEHDA	0.605	5	0.576	0.987	0.104	386.129	0.034	0.249	0.226	0.363	0.127
hα3β4 subtype											
CoMFA											
S	0.787	6	0.518	0.948	0.255	91.574	1				
E	0.830	6	0.462	0.969	0.197	157.454		1			
SE	0.934	6	0.288	0.985	0.139	319.679	0.512	0.488			
CoMSIA											
SE	0.945	6	0.262	0.988	0.125	399.560	0.152	0.848			
SEH	0.688	6	0.627	0.979	0.162	234.901	0.084	0.529	0.387		
SED	0.900	6	0.354	0.975	0.179	191.750	0.061	0.426		0.513	
SEA	0.871	6	0.402	0.976	0.174	202.120	0.148	0.773			0.079
SEDA	0.868	5	0.408	0.972	0.189	171.724	0.057	0.404		0.484	0.055
SEHD	0.717	4	0.600	0.981	0.154	259.610	0.038	0.306	0.204	0.452	
SEHA	0.669	6	0.645	0.975	0.176	197.341	0.074	0.368	0.367		0.190
SEHDA	0.749	4	0.571	0.983	0.147	287.861	0.034	0.216	0.232	0.388	0.129

*Fields used, S=steric, E=electrostatic, H=hydrophobics, D=H-bond donor, A=H-bond acceptor; †q^2, cross-validated correlation coefficient from leave-one-out (LOO); ‡N, optimum number of components; §SEP, standard error of prediction; ‖r^2_{ncv}, non-cross-validated correlation coefficient; ¶SEE, standard error of estimate; **F, F-test value.

Table 4. CoMSIA actual and predicted activity (pEC_{50}) of the training set

No	hα4β2 subtype			hα3β4 subtype			No	hα4β2 subtype			hα3β4 subtype		
	Actual	Predicted	Residuals	Actual	Predicted	Residuals		Actual	Predicted	Residuals	Actual	Predicted	Residuals
1	7.15	7.37	−0.22	7.32	7.17	0.15	20	6.96	7.04	−0.08	6.08	6.00	0.08
2	6.48	6.54	−0.06	6.59	6.54	0.05	21	7.68	7.73	−0.05	8.10	8.22	−0.12
3	7.89	7.86	0.03	7.54	7.73	−0.19	22	6.44	6.39	0.05	6.80	6.79	0.01
4	7.62	7.78	−0.16	7.60	7.36	0.24	23	8.21	8.00	0.21	8.36	8.24	0.12
5	6.82	6.63	0.19	7.12	7.29	−0.17	24	6.39	6.41	−0.02	5.77	5.63	0.14
6	6.00	6.07	−0.07	6.02	6.11	−0.09	25	7.43	7.60	−0.17	5.86	5.89	−0.03
7	7.92	8.03	−0.11	8.00	8.15	−0.15	26	6.67	6.71	−0.04	5.82	5.80	0.02
8	8.11	7.84	0.27	8.09	7.91	0.18	27	6.75	6.90	−0.15	6.47	6.58	−0.11
9	7.12	7.05	0.07	6.96	7.05	−0.09	28	6.87	6.95	−0.08	6.53	6.52	0.01
10	8.14	8.09	0.05	8.14	8.06	0.08	29	6.70	6.58	0.12	6.69	6.73	−0.04
11	7.33	7.29	0.04	7.15	7.20	−0.05	30	5.66	5.90	−0.24	5.59	5.53	0.06
12	5.72	5.72	0.00	6.31	6.20	0.11	31	5.71	5.92	−0.21	5.25	5.42	−0.17
13	6.89	6.92	−0.03	6.74	6.56	0.18	32	6.96	7.02	−0.06	6.10	6.08	0.02
14	5.57	5.60	−0.03	5.35	5.41	−0.06	33	6.76	6.73	0.03	6.62	6.63	−0.01
15	5.66	5.56	0.10	5.96	6.17	−0.21	34	5.83	5.78	0.05	4.63	4.51	0.12
16	5.30	5.32	−0.02	5.62	5.58	0.04	35	6.47	6.54	−0.07	5.13	5.16	−0.03
17	6.21	6.20	0.01	6.91	6.94	−0.03	36	5.11	5.06	0.05	4.20	4.28	−0.08
18	5.87	5.64	0.23	5.55	5.66	−0.11	37	5.96	5.98	−0.02	5.36	5.28	0.08
19	6.19	6.14	0.05	5.85	5.83	0.02							

the model. The best predictive model gives 6 as optimum number of components, and 12.8% and 87.2%, as the relative contributions of steric field and electrostatic field, respectively, showing a strong influence of the electrostatic interaction in activity. For hα3β4 subtype model, CoMSIA (0.945) with steric and electrostatic fields showed better q2 value than from CoMFA (0.934). A good predictivity of the model is suggested by the q^2 (0.945) and the r^2_{ncv} (0.988) coefficient values. The optimum number of components are 6, and the relative contributions of steric field (15.2%) and electrostatic field (84.8%) suggested a strong electrostatic interaction in activity.

The actual and predicted activities in the training set are described in Table 4. The small residual values indicate that the calculated activities from CoMSIA model are correlated well with actual activity. The test set with 7 compounds was used to validate the predictivity of CoMSIA model, and they were computed and treated by the same method as in training set. The activity of test set was predicted and compared with actual activity, which is shown in Table 5. The predicted values of test set were also correlated well with actual values.

Table 5. CoMSIA actual and predicted activity (pEC_{50}) of the test set

No	hα4β2 subtype			hα3β4 subtype		
	Actual	Predicted	Residuals	Actual	Predicted	Residuals
T1	7.09	7.05	0.04	6.96	7.05	−0.09
T2	5.72	5.85	−0.13	6.00	5.82	0.18
T3	7.00	7.00	0.00	6.41	6.60	−0.19
T4	6.74	6.55	0.19	5.24	5.26	−0.02
T5	5.85	5.70	0.15	5.81	5.98	−0.17
T6	7.12	7.11	0.01	5.72	5.95	−0.23
T7	5.77	5.77	0.00	5.53	5.37	0.16

DISCUSSION

The CoMSIA contour maps of steric and electrostatic field for hα4β2 subtype and hα3β4 subtype model are shown in Fig. 2, 3, 4, and 5, respectively. In the steric fields, sterically favorable areas are shown in green and sterically unfavorable areas are shown in yellow. In the electrostatic fields, the positively charged groups are favorable in blue regions and the negatively charged groups are favorable in red regions. The molecule in CoMSIA contour maps was compound (23) which showed the most potent activity.

For hα4β2 subtype model in Fig. 2, the sterically favored green regions are close to C_1, C_4, and R_1 positions. The sterically unfavored yellow regions are spaced near the N_8, R_2,

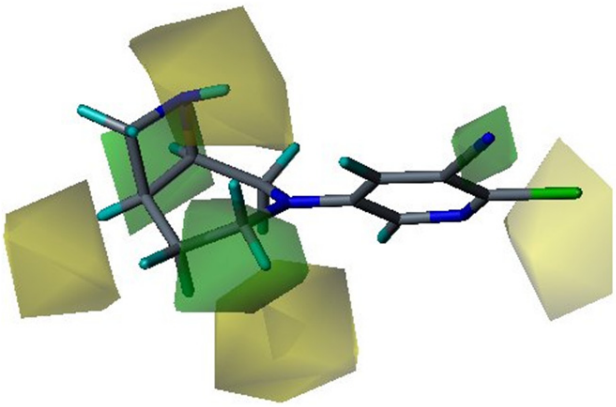

Fig. 2. CoMSIA contour map of steric field for the hα4β2 subtype.

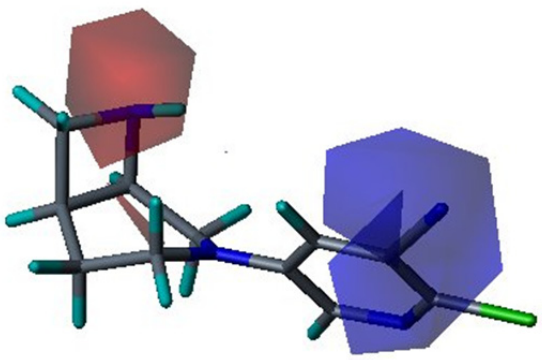

Fig. 3. CoMSIA contour map of electrostatic field for the hα4β2 subtype.

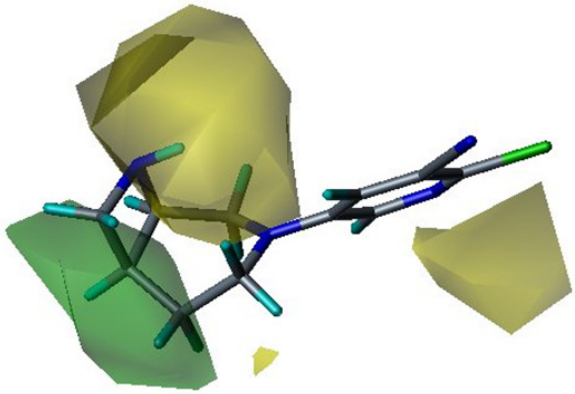

Fig. 4. CoMSIA contour map of steric field for the hα3β4 subtype.

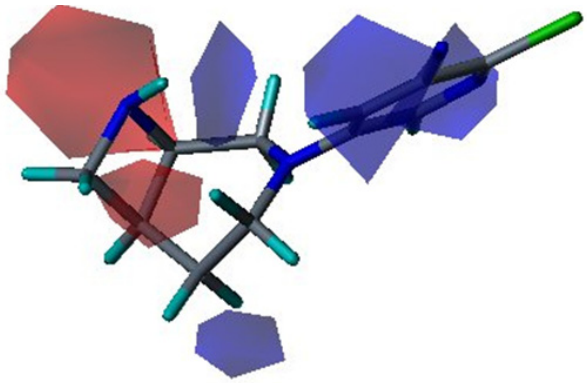

Fig. 5. CoMSIA contour map of electrostatic field for the hα3β4 subtype.

C_5-C_6 and N_3 positions. For h$\alpha 3\beta 4$ subtype in Fig. 4, one green contour was found near the C_5-C_6 area, and two yellow contours were shown at the upper side of N_8-C_1-C_2-C_3 region and in the vicinity of R_1 substitution.

For h$\alpha 4\beta 2$ subtype model in Fig. 3, the positive charge favorable blue regions are close to pyridine ring and R_1 positions, whereas the negative charge favorable red region is located near the N_8 position. In h$\alpha 3\beta 4$ subtype of Fig. 5, the four blue contours are found around the pyridine ring, R_1, C_5 and C_1-C_2 regions. The two red contours near the C_6 and at N_8 positions are negative charge favorable regions.

In conclusion, therefore, small groups at C_1, C_4 and R_1, hydrogen at C_5, and negative charge atom at C_6 positions in 3-N-substituted diazabicyclo[4.2.0]octanes are showen to enhance the activity for h$\alpha 4\beta 2$ subtype while reducing the activity for h$\alpha 3\beta 4$ subtype.

ACKNOWLEDGMENTS

This Research was supported by Chung-Ang University Research Scholarship Grants in 2007-2008.

REFERENCES

Cashin AL, Torrice MM, McMenimen KA, Lester HA, Dougherty DA. Chemical-scale studies on the role of a conserved aspartate in preorganizing the agonist binding site of the nicotinic acetylcholine receptor. *Biochemistry* 46: 630−639, 2007

Dehkordi O, Millis RM, Dennis GC, Jazini E, Williams C, Hussain D, Jayam-Trouth A. Expression of α-7 and α-4 nicotinic acetylcholine receptors by GABAergic neurons of rostral ventral medulla and caudal pons. *Brain Res* 1185: 95−102, 2007

Dougherty JJ, Wu J, Nichols RA. β-Amyloid regulation of presynaptic nicotinic receptors in rat hippocampus and neocortex. *J Neurosci* 23: 6740−6747, 2003

Frost MJ, Bunnelle HW, Tietje KR, Anderson DJ, Rueter LE, Curzon P, Surowy CS, Jerome JJ, Kohlhaas DK, Buckley MJ, Henry RF, Dyhring T, Ahring PK, Meyer MD. Synthesis and structure-activity relationships of 3,8-diazabicyclo[4.2.0]octane ligands, potent nicotinic acetylcholine receptor agonists. *J Med Chem* 49: 7843−7853, 2006

Girod R, Barazangi N, McGehee D, Role LW. Facilitation of glutamatergic neurotransmission by presynaptic nicotinic acetylcholine receptors. *Neuropharmacology* 39: 2715−2725, 2000

Gotti C, Zoli M, Clementi F. Brain nicotinic acetylcholine receptors: native subtypes and their relevance Trends. *Pharmacol Sci* 27: 482−491, 2006

Grady SR, Salminen O, Laverty DC, Whiteaker P, McIntosh JM, Collins AC, Marks MJ. The subtypes of nicotinic acetylcholine receptors on dopaminergic terminals of mouse striatum. *Biochem Pharmacol* 74: 1235−1246, 2007

Hays JT, Ebbert J, Sood A. Efficacy and safety of varenicline for smoking cessation. *Am J Med* 121: S32−S42, 2008

Hogg RC, Bertrand D. Neuroscience: What genes tell us about nicotine addiction. *Science* 306: 983−985, 2004

Jensen AA, Frølund B, Liljefors T, Krogsgaard LP. Neuronal nicotinic acetylcholine receptors: structural revelations, target identifications, and therapeutic inspirations. *J Med Chem* 48: 4705−4745, 2005

Kenny PJ, File SE, Neal MJ. Evidence for a complex influence of nicotinic acetylcholine receptors on hippocampal serotonin release. *J Neurochem* 75: 2409−2414, 2000

Kuryatov A, Onksen J, Lindstrom J. Roles of accessory subunits in α4β2 nicotinic receptors. *Molecular Pharmacology* 74: 132−143, 2008

Lape R, Colquhoun D, Sivilotti LG. On the nature of partial agonism in the nicotinic receptor superfamily. *Nature* 454: 722−727, 2008

O'Leary KT, Parameswaran N, Johnston LC, McIntosh JM, Di Monte DA, Quik M. Paraquat exposure reduces nicotinic receptor-evoked dopamine release in monkey striatum. *J Pharmacol Exp Ther* 327: 124−129, 2008

Owen RT, Serradell N, Rosa E. Ispronicline: nicotinic acetylcholine α4β2 agonist treatment of cognition disorders. *Drugs of the Future* 33: 197−202, 2008

Pons S, Fattore L, Cossu G, Tolu S, Porcu E, McIntosh JM, Changeux JP, Maskos U, Fratta W. Crucial role of α4 and α6 nicotinic acetylcholine receptor subunits from ventral tegmental area in systemic nicotine self-administration. *J Neurosci* 28: 12318−12327, 2008

Vincler M, McIntosh JM. Targeting the α9 α10 nicotinic acetylcholine receptor to treat severe pain. *Expert Opinion on Therapeutic Targets* 11: 891−897, 2007

SYBYL Molecular Modeling Software. Tripos Inc., St. Louis, USA, 2008